Article

Neuron

Erythrocytes Are Oxygen-Sensing Regulators of the Cerebral Microcirculation

Highlights

- Activity-dependent cortical hyperemia begins in capillaries
- Transient dips in tissue O_2 tension drive capillary hyperemia
- Depletion of O_2 increases isolated erythrocyte flow velocity ex vivo
- Erythrocytes are O_2 sensors that regulate their own deformability and flow velocity

Authors

Helen Shinru Wei, Hongyi Kang, Izad-Yar Daniel Rasheed, ..., Chris Xu, Jiandi Wan, Maiken Nedergaard

Correspondence

jdween@rit.edu (J.W.), nedergaard@urmc.rochester.edu (M.N.)

In Brief

Wei et al. demonstrate a novel mechanism for cerebral capillary blood flow regulation. Erythrocytes increase their deformability in response to decreases in oxygen tension resulting in an autonomous increase in capillary flow velocities and rapid rise in oxygen supply.

Wei et al., 2016, Neuron *91*, 1–12
August 17, 2016
http://dx.doi.org/10.1016/j.neuron.2016.07.016

CellPress

Please cite this article in press as: Wei et al., Erythrocytes Are Oxygen-Sensing Regulators of the Cerebral Microcirculation, Neuron (2016), http://dx.doi.org/10.1016/j.neuron.2016.07.016

Neuron
Article

Erythrocytes Are Oxygen-Sensing Regulators of the Cerebral Microcirculation

Helen Shinru Wei,[1] Hongyi Kang,[1] Izad-Yar Daniel Rasheed,[2] Sitong Zhou,[3] Nanhong Lou,[1] Anna Gershteyn,[1] Evan Daniel McConnell,[1] Yixuan Wang,[3,4] Kristopher Emil Richardson,[5] Andre Francis Palmer,[5] Chris Xu,[6] Jiandi Wan,[3,*] and Maiken Nedergaard[1,7,*]

[1]Center for Translational Neuromedicine, University of Rochester Medical Center, Rochester, NY 14642, USA
[2]Department of Neurology, Northwestern University Feinberg School of Medicine, Chicago, IL 60611, USA
[3]Department of Microsystems Engineering, Rochester Institute of Technology, Rochester, NY 14623, USA
[4]School of Mechanical Engineering, University of Science and Technology, Beijing 100083, China
[5]William G. Lowrie Department of Chemical & Biomolecular Engineering, The Ohio State University, Columbus, OH 43210, USA
[6]School of Applied & Engineering Physics, Cornell University, Ithaca, NY 14853, USA
[7]Center for Basic and Translational Neuroscience, Faculty of Health and Medical Sciences, University of Copenhagen, 2200 Copenhagen, Denmark
*Correspondence: jdween@rit.edu (J.W.), nedergaard@urmc.rochester.edu (M.N.)
http://dx.doi.org/10.1016/j.neuron.2016.07.016

SUMMARY

Energy production in the brain depends almost exclusively on oxidative metabolism. Neurons have small energy reserves and require a continuous supply of oxygen (O_2). It is therefore not surprising that one of the hallmarks of normal brain function is the tight coupling between cerebral blood flow and neuronal activity. Since capillaries are embedded in the O_2-consuming neuropil, we have here examined whether activity-dependent dips in O_2 tension drive capillary hyperemia. In vivo analyses showed that transient dips in tissue O_2 tension elicit capillary hyperemia. Ex vivo experiments revealed that red blood cells (RBCs) themselves act as O_2 sensors that autonomously regulate their own deformability and thereby flow velocity through capillaries in response to physiological decreases in O_2 tension. This observation has broad implications for understanding how local changes in blood flow are coupled to synaptic transmission.

INTRODUCTION

Neurovascular coupling is a process in which synaptic activity is linked to local changes in cerebral blood flow (Iadecola and Nedergaard, 2007; Kleinfeld et al., 2011). The mechanisms by which neural activity triggers hyperemia have been extensively studied because neurovascular coupling forms the basis for functional brain imaging. In addition, defects in neurovascular coupling may contribute to cognitive decline in neurodegenerative diseases, such as Alzheimer disease, as well as in hypertension and stroke (Girouard and Iadecola, 2006). Functional hyperemia can be mediated by a number of compounds, many of which are by-products of neural activity, including adenosine, nitric oxide (NO), prostaglandin E_2 (PGE_2), potassium ions (K^+), epoxyeicosatrienoic acids (EETs), and carbon dioxide (CO_2) (Iadecola and Nedergaard, 2007). In addition, functional hyperemia is preceded by a transient decrease in tissue oxygenation (Devor et al., 2011; Lecoq et al., 2011; Parpaleix et al., 2013). Since recent work has documented that functional hyperemia is initiated in microvessels embedded in the oxygen (O_2)-consuming neuropil, we asked whether the initial dip in tissue O_2 tension drives brain capillary hyperemia.

RESULTS

Functional Hyperemia Begins in Capillaries and Is Inhibited When Oxidative Phosphorylation Is Suppressed

To identify the brain region activated by hindlimb stimulation, we first visualized the exposed cortex using intrinsic optical signaling (IOS) followed by high-speed two-photon line scanning to assess red blood cell (RBC) velocities in arterioles and capillaries in the contralateral sensory cortex of lightly sedated mice (Figure 1A) (Bekar et al., 2012; Takano et al., 2006). Only cortical arterioles and capillaries located in the cortical region that exhibited the largest activity-dependent increase in IOS were analyzed. A comparison of the onset time of stimulation-induced elevation in RBC velocity revealed that capillary RBC velocities (0.67 ± 0.15 s, n = 65, 25 mice) increased prior to RBC velocities of upstream arterioles (2.33 ± 0.22 s, n = 61, 25 mice) (Figure 1B), which is consistent with conclusions drawn by a prior study on vascular diameters (Hall et al., 2014). Additional analysis of a subset of connected capillaries and arterioles confirmed that, following hindlimb stimulation, the onset of RBC velocity increases in capillaries preceded that of upstream arterioles (Figure S1A). In these experiments, cortical vascular trees were mapped prior to data collection and corresponding arterioles and capillaries were identified for line scanning. We also collected line scans orthogonally across vessel widths of arterioles and capillaries. These data showed that arterioles dilated at 2.38 ± 0.37 s, whereas capillary dilation occurred at 2.46 ± 0.22 s after hindlimb stimulation (n = 53–283, 15–18 mice) (Figure 1C). In agreement with a recent publication, a slight dilation of capillaries was noted, but this occurred concomitant with arteriole dilation and most likely reflected pressure-induced increases in blood flow and/or

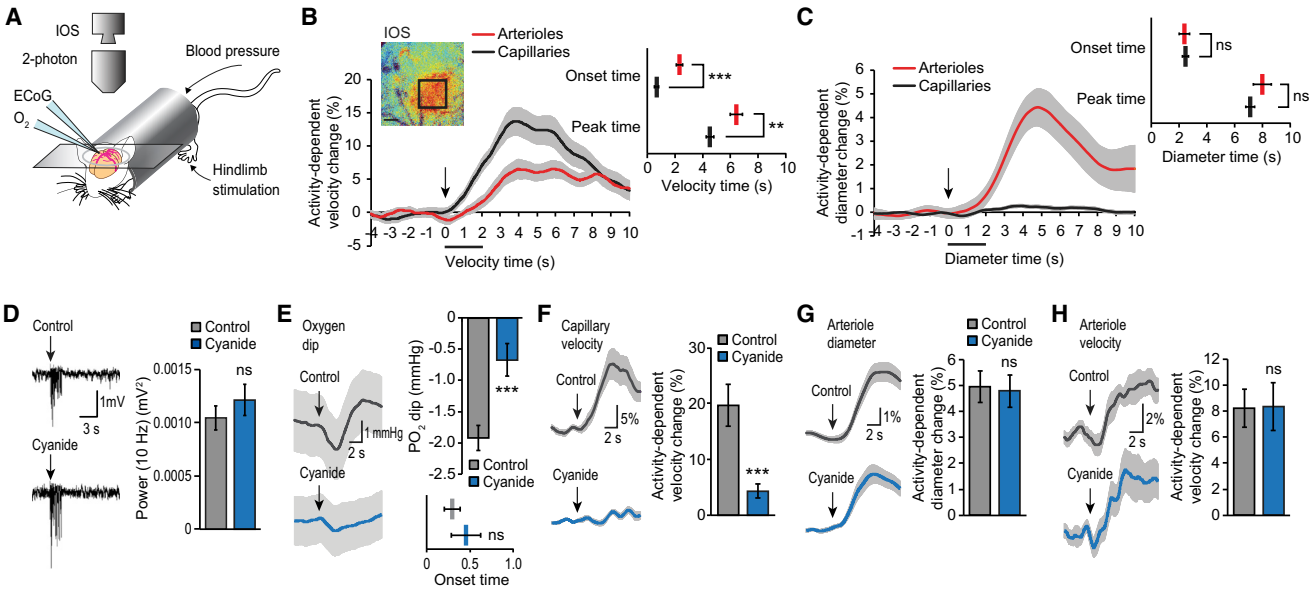

Figure 1. PO_2 Dips Are Necessary to Elicit Capillary Hyperemia

(A) Experimental setup for assessing functional hyperemia elicited by sensory stimulation. Arterial blood pressure was monitored through a femoral artery catheter while the other hindlimb was stimulated. Through a cranial window, intrinsic optical signaling (IOS) was used to identify the cortical region of functional hyperemia. LFP and O_2 sensor microelectrodes were placed in close proximity (10–20 μm) to one another within the activated region. During hindlimb stimulation, blood vessels in the activated contralateral hindlimb cortex were imaged using two-photon laser scanning microscopy.

(B) Time-course plot of hindlimb stimulation-evoked RBC velocity changes in cortical arterioles (red) and capillaries (black). Inset: IOS imaging (shown as a pseudocolor image) was used to identify the location of the activated hindlimb cortex in all experiments. Scale bar, 300 μm. Evoked RBC velocity increases began in capillaries (0.67 ± 0.15 s) prior to arterioles (2.33 ± 0.22 s). n = 61–65, 25 mice. ***p < 0.001, t test; **p < 0.01, Mann-Whitney test. Black arrow indicates start of stimulation, black bar indicates duration of stimulation.

(C) Time-course plot of diameter changes of cortical arterioles (red) and capillaries (black). Arterioles began to dilate at 2.38 ± 0.37 s and capillaries at 2.46 ± 0.22 s after hindlimb stimulation. n = 53–283, 15–18 mice. ns, p > 0.05, Mann-Whitney test.

(D) Topical treatment with cyanide (100 μM) did not alter LFP power within the duration of the experiments. n = 13, 5 mice. ns, p > 0.05, paired t test.

(E) Activity-dependent PO_2 dips were suppressed by cyanide (1.92 ± 0.20 mmHg PO_2 dip without NaCN, 0.67 ± 0.26 mmHg PO_2 dip with NaCN). n = 36–47, 4–21 mice. ***p < 0.001, Mann-Whitney test. Onset of the evoked PO_2 dip was unchanged by cyanide (0.29 ± 0.09 s without NaCN, 0.46 ± 0.17 s with NaCN). n = 36–47, 4–21 mice. ns, p > 0.05, Mann-Whitney test.

(F) Activity-dependent increases in capillary RBC velocity was nearly abolished by cyanide (19.66% ± 3.83% without NaCN, 4.29% ± 1.20% with NaCN). n = 29–38, 6–13 mice. ***p < 0.001, t test.

(G) Activity-dependent penetrating arteriole vasodilation was unaffected by cyanide (4.95% ± 0.61% without NaCN, 4.79% ± 0.61% with NaCN). n = 66–79, 13–17 mice. ns, p > 0.05, Mann-Whitney test.

(H) Activity-dependent increases in cortical arteriole RBC velocity persisted in the presence of cyanide (8.22% ± 1.47% without NaCN, 8.36% ± 1.85% with NaCN). n = 35–43, 18–19 mice. ns, p > 0.05, Mann-Whitney test. Data are represented as mean ± SEM.

See also Figure S1.

volume (Hill et al., 2015). Thus, activity-dependent increases in capillary RBC velocities occur prior to both dilations of and RBC velocity increases in upstream arterioles, indicating that capillary hyperemia occurs before arterial hyperemia.

An intraparenchymal dip in partial pressure of oxygen (PO_2) (Yacoub et al., 2001) began at 0.29 ± 0.09 s after hindlimb stimulation (Figure 1E), similar to previous reports (Lecoq et al., 2011; Parpaleix et al., 2013), and thereby preceded capillary hyperemia by as much as 0.38 s. Could the transient dip in tissue PO_2 be responsible for the initial phase of capillary hyperemia? To test this question, we applied sodium cyanide (NaCN), a potent inhibitor of cytochrome *c* oxidase and thus O_2 utilization, to the exposed cerebral cortex. Initial experiments showed that 0.1 mM NaCN was the highest concentration that did not interfere with excitatory potentials evoked by hindlimb stimulation (Figure 1D). Applying 0.1 mM NaCN on the pial surface increased resting PO_2 (18.62 ± 2.51 mmHg PO_2 before NaCN, 38.74 ± 4.40 mmHg PO_2 after NaCN, n = 10 mice, p < 0.0001, paired t test). NaCN also significantly suppressed stimulation-induced dips in tissue PO_2, though it did not change the onset of the evoked PO_2 dip (Figure 1E). NaCN reduced the amplitude of capillary hyperemia by 78% (n = 29–38, 6–13 mice, p < 0.001, t test) (Figure 1F), but it did not attenuate activity-evoked penetrating arteriole vasodilation or velocity increases (Figures 1G and 1H). This observation is surprising because the release of traditional smooth muscle relaxing mediators of functional hyperemia, including adenosine and K^+, is potentiated rather than inhibited when oxidative phosphorylation is suppressed (Daval et al., 1980). The fact that NaCN application significantly suppressed capillary hyperemia alone is consistent with the idea that the activity-induced transient dip in tissue PO_2 triggers an increase in local capillary RBC velocity.

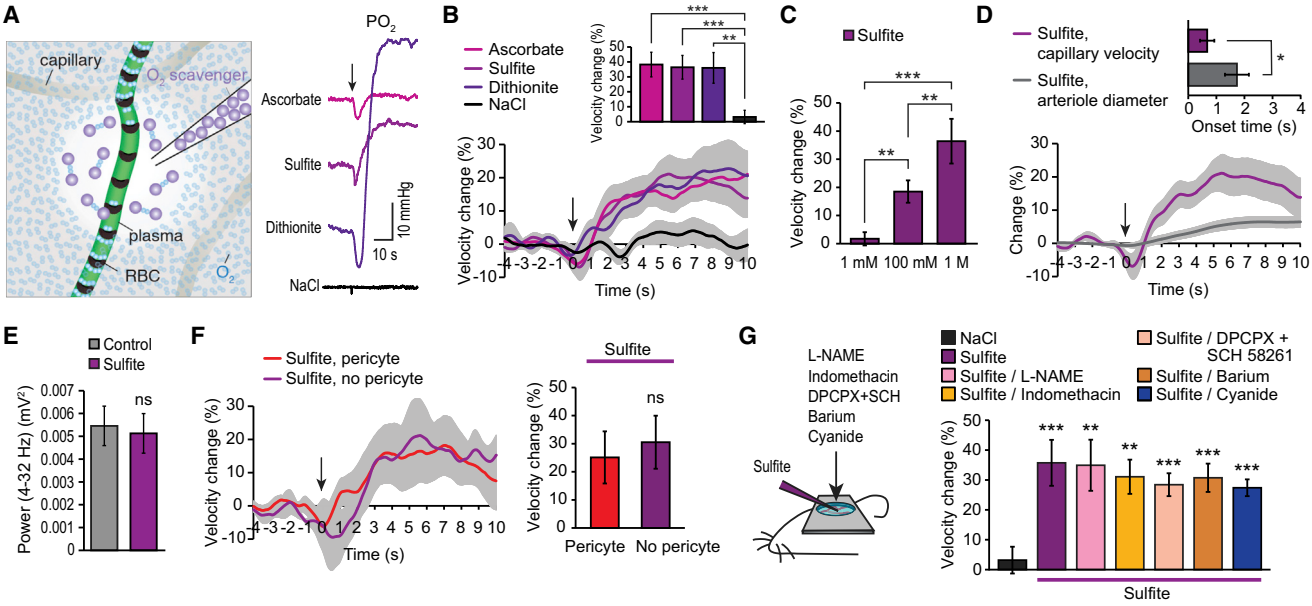

Figure 2. PO_2 Dips Are Sufficient to Elicit Capillary Hyperemia

(A) Left: experimental setup used to study the effect of local application of O_2 scavengers (sodium ascorbate, sulfite, or dithionite, 1 M). The O_2 scavengers were delivered by a micropipette inserted 100–150 μm below the pial surface and placed <50 μm from a capillary. Upon microinjection, O_2 molecules within the vicinity of the pipette tip were trapped by the scavenger, resulting in a transient drop in local O_2 tension. Right: local tissue PO_2 was measured by an O_2 sensor placed <50 μm from the scavenger pipette tip and displayed a transient reduction in O_2 tension followed by a PO_2 overshoot. Black arrow indicates time of microinjection.

(B) Nearby capillary RBC velocity increased robustly after microinjection of any of the O_2 scavengers: ascorbate, sulfite, or dithionite. Inset: a summary histogram of capillary RBC velocity changes induced by the transient reduction in tissue O_2 tension. n = 23–34, 6–12 mice. **p < 0.01, ***p < 0.001, Kruskal-Wallis with Dunn's test.

(C) Increasing the concentration of sulfite microinjected in close proximity to a capillary increased RBC velocity in a dose-dependent manner. n = 34–91, 4–12 mice. **p < 0.01, ***p < 0.001, Kruskal-Wallis with Dunn's test.

(D) Sulfite microinjection (1 M) near penetrating arterioles resulted in arteriole vasodilation that was delayed relative to capillary velocity increases. n = 19–34, 5–12 mice. *p < 0.05, t test.

(E) Sulfite microinjection (1 M) did not alter neuronal activity (LFPs) detected at a distance of <50 μm from the sulfite pipette tip. n = 21, 4 mice. ns, p > 0.05, paired t test.

(F) Local sulfite microinjection increased RBC velocity in both capillaries with pericytes and without pericytes identified in NG2-DsRed reporter mice. n = 5–8, 6 mice. ns, p > 0.05, t test. Purple bar indicates sulfite microinjection groups.

(G) Left: inhibitors were topically applied to the cranial window prior to microinjection of sulfite. Right: a summary histogram of capillary RBC velocity changes induced by sulfite microinjection in the presence of the nitric oxide synthase (NOS) inhibitor L-NAME (2 mM), cyclooxygenase (COX) inhibitor indomethacin (500 μM), adenosine receptor inhibitors DPCPX and SCH 58261 (each 1 μM), K^+ channel inhibitor barium (100 μM), and cytochrome *c* oxidase inhibitor cyanide (100 μM). n = 27–47, 5–6 mice. **p < 0.01, ***p < 0.001, compared to saline, Kruskal-Wallis with Dunn's test. Data are represented as mean ± SEM.

See also Figure S2.

PO_2 Dips Are Sufficient to Elicit Capillary Hyperemia

We next asked whether a change in tissue PO_2, in the absence of sensory activation, is sufficient to trigger capillary hyperemia. To address this question, we separately microinjected three structurally different O_2 scavengers, sodium ascorbate, sodium sulfite, or sodium dithionite, near capillaries in the hindlimb cortex under the guidance of two-photon imaging (Figure 2A). Ascorbate, sulfite, and dithionite all triggered a rapid decrease in local tissue PO_2. Similar to activity-dependent responses, tissue PO_2 exhibited a bi-phasic pattern, with an initial transient dip followed by a delayed and long-lasting overshoot (Figure 2A). Strikingly, RBC velocity increased in nearby capillaries after microinjection of O_2 scavengers, suggesting that tissue oxygenation influences capillary blood flow (Figure 2B). For more detailed analyses, we focused on sulfite, which is converted to the relatively non-toxic compound sulfate after reaction with O_2. We found that increasing the concentration of sulfite triggered a dose-dependent increase in RBC velocity (Figure 2C). Sulfite microinjection also caused vasodilation of nearby penetrating arterioles, but the arteriolar vasodilation was delayed relative to sulfite-induced capillary velocity increases (Figure 2D). Microinjection of the maximal concentration of sulfite (1 M) was not associated with detectable changes in the power spectrum of local field potential (LFP) activity (Figure 2E). Thus, local application of O_2 scavengers alone in the absence of sensory stimulation triggered hyperemia that closely resembled activity-dependent hyperemia. Moreover, sulfite elicited capillary hyperemia in both capillaries with and without pericytes in NG2-DsRed mice, suggesting that increases in RBC velocity occurred independent of pericyte presence (Figure 2F). We defined capillaries with pericytes as capillaries in contact with pericyte cell bodies and capillaries without pericytes as capillaries lacking contact with pericyte

cell bodies. Next, we asked whether it is the depletion of O_2 that directly triggers hyperemia or whether hyperemia is induced indirectly by release of vasoactive mediators. To systematically address this, we tested whether sulfite-elicited capillary hyperemia was reduced by pretreatment with inhibitors of NO production (L-NAME), inhibitors of PGE_2 production (indomethacin), adenosine A1 and A2A receptor antagonists (DPCPX and SCH 58261), or inhibitors of inward-rectifying K^+ channels (barium). Topical application of these inhibitors to the pial surface all failed to suppress sulfite-induced capillary hyperemia (Figure 2G), indicating that PO_2-induced capillary hyperemia is not dependent on vascular smooth muscle relaxation.

To evaluate the contribution of pericytes to capillary hyperemia, we compared the amplitude and onset time of activity-induced RBC velocity increases of capillaries in contact with pericyte cell bodies with capillaries lacking contact with pericyte cell bodies in NG2-DsRed reporter mice. The baseline capillary diameter adjacent to the cell bodies of NG2-DsRed pericytes did not differ from segments of capillaries not in contact with pericyte cell bodies (Figure S2A). We found that activity-evoked capillary hyperemia was unaffected by the presence or absence of an adjacent pericyte cell body. Capillary RBC velocity began at 0.71 ± 0.35 s in capillaries with pericytes (n = 28, 5 mice) and at 0.66 ± 0.22 s in capillaries without pericytes (n = 31, 5 mice) (Figure S2B). Next, we evaluated pericyte expression of actin in mouse cortex using phalloidin staining of F-actin as well as α-smooth muscle actin (α-SMA) immunolabeling in fixed sections. Similar to prior studies, we defined the penetrating vessel as the zeroth branch order vessel, with subsequent branches labeled using increasing branch order numbers (Hall et al., 2014; Hill et al., 2015; Kornfield and Newman, 2014). Quantification confirmed that vessels beyond the third branch order were largely phalloidin and α-SMA negative (only 1.4% of vessels fourth order or higher, averaging 4.0 μm in diameter, were phalloidin and/or α-SMA positive, n = 49 vessels from 9 mice). In contrast, vessel branches zero to three were largely phalloidin and/or α-SMA positive (22%–100% actin positive, ranging from 5.4 to 13.3 μm in diameter, n = 12–25 vessels from 9 mice) (Figure S2C). Only ~30% of DsRed+ pericyte cell bodies along branches one to three were actin positive (Figures S2D and S2E). These observations are in agreement with a recent study showing that smooth muscle actin is expressed by arterioles, but not capillary mural cells, in mouse and human neocortex (Hill et al., 2015). Hill et al. also showed that unlike smooth muscle actin-positive arterioles, pericyte-covered capillaries do not constrict or dilate in response to stimulation.

An important detail for validation of our in vivo analysis was our finding that 100% of DsRed-positive cells were PDGFRβ positive and conversely that 100% of PDGFRβ-positive cells were DsRed positive in NG2-DsRed reporter mice (Figure S2F). In addition, DsRed-positive perivascular cells in NG2-DsRed reporter mice stained positively for desmin and CD13 in immunohistochemical slices (Figure S2G). Therefore, capillaries identified as with or without pericytes during in vivo imaging of NG2-DsRed reporter mice were properly categorized, as PDGFRβ, desmin, and CD13 are pericyte-specific markers (Armulik et al., 2011).

AMPA Receptor Activity Modulates Capillary RBC Velocity

The velocity by which RBCs pass through capillaries is highly variable (Chaigneau et al., 2003; Kleinfeld et al., 1998; Stefanovic et al., 2008). Based on the observation of a tight coupling between postsynaptic AMPA receptor activity and tissue PO_2 (Enager et al., 2009; Mathiesen et al., 2011), as well as our observation that NaCN inhibits both evoked PO_2 dips and capillary hyperemia (Figure 1E and 1F) while microinjection of O_2 scavengers induces capillary hyperemia (Figure 2B), we asked whether the ever-changing pattern of synaptic activity contributes to spontaneous fluctuations in capillary RBC velocity.

The AMPA receptor antagonist CNQX (200 μM) was topically applied to the cerebral cortex and its effect on baseline (unstimulated) LFPs, PO_2, and capillary RBC velocity was assessed. As a measure of baseline variability, we compared the SD of LFPs, PO_2, and capillary RBC velocity before and after application of CNQX (Figures 3A–3C). As expected, CNQX potently suppressed both the power and the SD of baseline LFPs (Figure 3A). Baseline PO_2 levels also exhibited a significant increase (52.6% increase) and the variability of baseline PO_2 was reduced (45.0% suppression of SD by CNQX) (Figure 3B). Baseline capillary RBC velocity decreased by 25.7%, and interestingly, the SD of RBC velocity fluctuations also fell significantly in response to CNQX (26.7% suppression by CNQX) (Figure 3C), suggesting that AMPA receptor-mediated PO_2 dips in part contribute to the variability of capillary RBC velocity at rest. Prior analyses have shown that cardiac- and respiration-dependent pulsatile blood flow is also in part responsible for the high variability in baseline capillary RBC velocities (Santisakultarm et al., 2012). Of note, baseline arterial diameter remained unchanged after addition of CNQX (Figure 3D). To extend the analysis to include capillary functional hyperemia, we next compared responses to hindlimb stimulation before and after addition of CNQX. As expected, CNQX produced a dramatic decrease in excitatory potentials and PO_2 dip amplitudes evoked by a 2 s hindlimb stimulation (81.0% and 90.1% suppression by CNQX, respectively) (Figures 3E and 3F). Consistent with the key role of AMPA receptor activation in functional hyperemia, CNQX significantly delayed the onset and suppressed the amplitude of capillary RBC velocity increases in response to hindlimb stimulation (75.0% suppression by CNQX) (Figure 3G). Figures 3H and 3I compare the relative power by which blockade of AMPA receptors suppressed spontaneous fluctuations and stimulation-dependent changes in LFPs, PO_2, and capillary RBC velocity. Of note, inhibition of NMDA receptors (AP5, 500 μM) did not have a significant effect on capillary hyperemia (Figure S3). This observation is consistent with the idea that excitatory transmission is primarily the result of AMPA receptor activation in the sensory cortex (Hoffmeyer et al., 2007; Self et al., 2012).

Together, these results suggest that O_2-consuming synaptic activity is partly responsible for the variability of cortical capillary RBC velocities during resting conditions and primarily responsible for the initiation of activity-dependent capillary hyperemia.

Oxygen Depletion Alone Is Sufficient to Increase RBC Velocity Ex Vivo

The observation that microinjection of O_2 scavengers induced pericyte- and vasoactive mediator-independent capillary

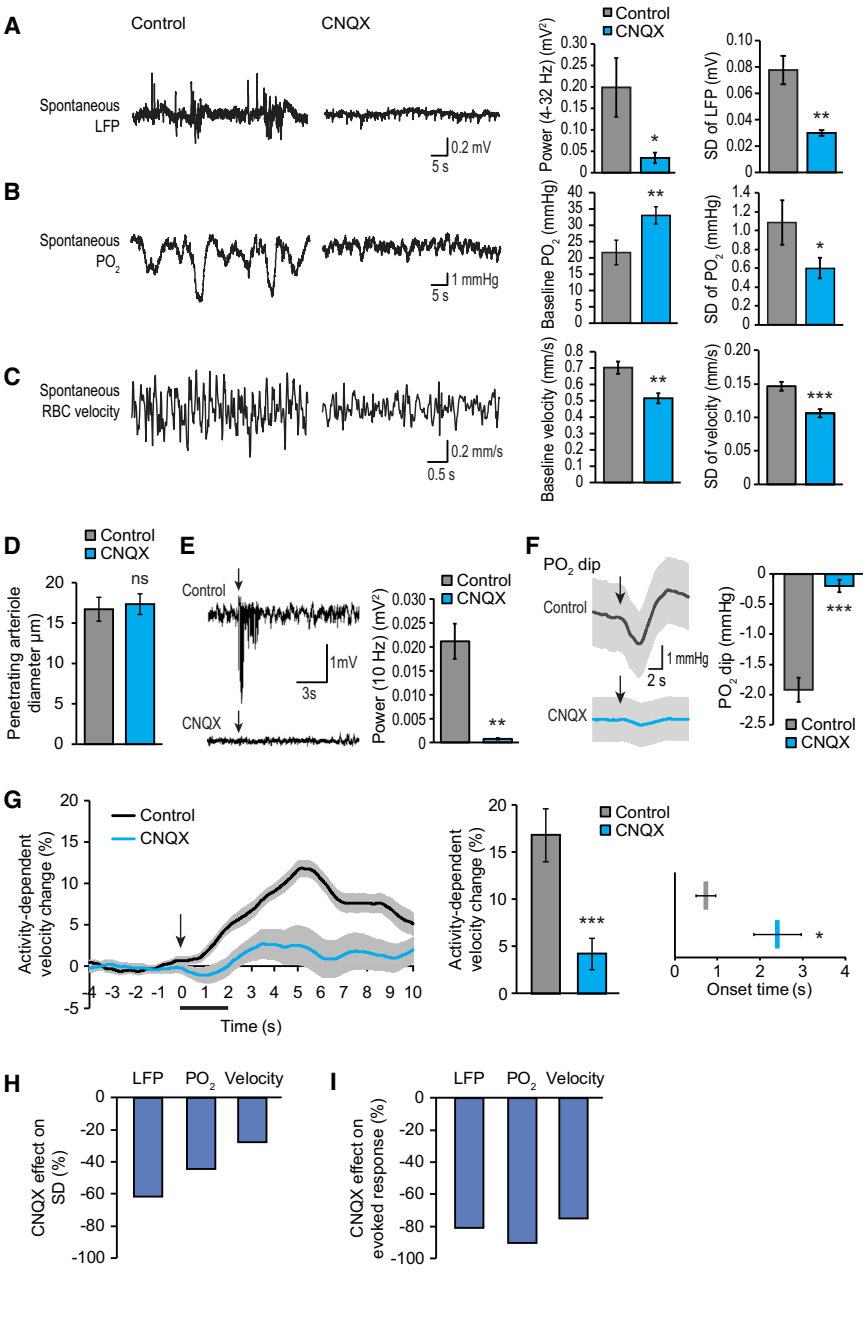

Figure 3. Capillary RBC Velocity Is Modulated by AMPA Receptor Activity

The AMPA receptor inhibitor CNQX (200 µM) was added to the artificial cerebrospinal fluid (aCSF) covering the cranial window for 30–45 min and recordings with and without CNQX were compared.

(A) Comparison of spontaneous (unstimulated) LFP activity (power at 4–32 Hz), as well as SD of spontaneous LFP activity before and after CNQX. n = 6 mice. *p < 0.05, **p < 0.01, t test.

(B) Comparison of baseline PO_2 level and the spontaneous variability (SD) of PO_2 before (21.65 ± 3.77 mmHg baseline and 1.09 ± 0.24 mmHg SD) and after (33.03 ± 2.64 mmHg baseline and 0.60 ± 0.11 mmHg SD) CNQX. n = 6–8 mice. **p < 0.01, *p < 0.05, paired t test.

(C) Comparison of baseline capillary RBC velocity and the spontaneous variability of RBC velocity before (0.70 ± 0.04 mm/s baseline and 0.15 ± 0.007 mm/s SD) and after (0.52 ± 0.03 mm/s baseline and 0.11 ± 0.006 mm/s SD) CNQX. n = 131–191, 12–13 mice. **p < 0.01, ***p < 0.001, Mann-Whitney test.

(D) CNQX did not alter the baseline diameters of penetrating arterioles (16.71 ± 1.48 µm before CNQX, 17.35 ± 1.28 µm after CNQX). n = 30, 7 mice. ns, p > 0.05, Wilcoxon test.

(E) Comparison of excitatory potentials evoked by hindlimb stimulation quantified as the LFP power at 10 Hz before and after CNQX. n = 15–23, 3–4 mice. **p < 0.01, t test. Black arrow indicates start of stimulation.

(F) Hindlimb stimulation-induced PO_2 dips were suppressed by CNQX (1.92 ± 0.20 mmHg in controls, 0.19 ± 0.10 mmHg after CNQX). n = 29–47, 9–21 mice. ***p < 0.001, Mann-Whitney test.

(G) Activity-dependent increases in capillary RBC velocity were reduced by CNQX. Bar histograms compare activity-induced capillary RBC velocity increases and onset times without (16.76% ± 2.76% increase and 0.73 ± 0.23 s onset) and with (4.19% ± 1.68% increase and 2.41 ± 0.56 s onset) CNQX. n = 49–54, 10–13 mice. ***p < 0.001, *p < 0.05, Mann-Whitney test. Black arrow indicates start of stimulation, black bar indicates duration of stimulation.

(H) Suppression of spontaneous variability in LFPs, PO_2, and capillary RBC velocity before and after CNQX as measured by SD.

(I) Suppression of activity-induced changes in LFPs, PO_2 dip, and capillary RBC velocity by CNQX. Data are represented as mean ± SEM.

See also Figure S3.

hyperemia led us to hypothesize that O_2 tension itself, independent of the neurovascular unit, can control RBC deformation and thus RBC flow through capillaries. To test this idea in the absence of the neurovascular unit, we turned to an ex vivo assessment of the effect of oxygenation on RBC flow through an artificial capillary. We employed a microfluidic device in which isolated human RBCs pass through a narrow flow channel (Figure 4A) (Abkarian et al., 2006; Cinar et al., 2015; Wan et al., 2008, 2011). This approach allowed an evaluation of RBC velocity in the absence of the cellular components of the neurovascular unit, i.e., endothelial cells, pericytes, and astrocytes (Petzold and Murthy, 2011). Since the capillary lumen is considerably smaller than RBC diameters, RBC deformability is a major determinant of the speed by which the RBC passes through a capillary (Chaigneau et al., 2003). A microfluidic device made of polydimethylsiloxane (PDMS) was submerged in a chamber containing sodium sulfite, an O_2 scavenger. Since PDMS is O_2, but not H_2O, permeable the chamber functioned as a sink for O_2 (Figure 4A). A colorimetric calibration, based on adding the O_2-sensing dye tris(2,2′-bipyridyl)dichlororuthenium(II) hexahydrate to deionized (DI) water showed that PO_2 in the flow channel was an inverse function of the sulfite concentration (0 to 2 M)

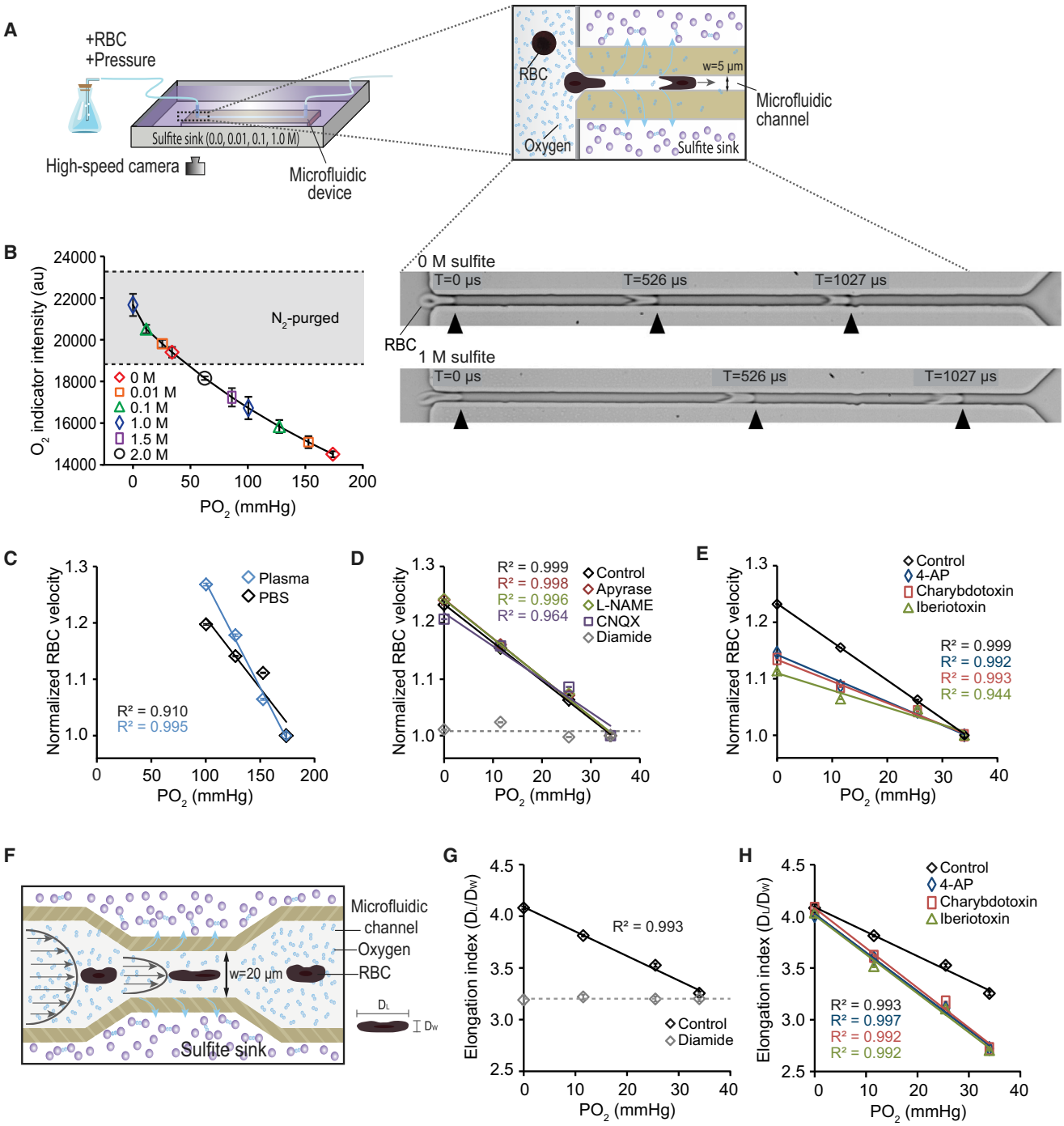

Figure 4. Oxygen Depletion Alone Is Sufficient to Increase RBC Velocity Ex Vivo

(A) A diagram of the experimental setup for ex vivo analysis of the effect of PO_2 on RBC flow velocity. Human RBCs (~7 μm in diameter) were added to the bath containing PBS and forced to flow through a microfluidic device containing a narrow channel (5 μm) by applying a constant pressure (1.6 psi). The microfluidic device was submerged in an O_2 sink (chamber containing H_2O with 0.0, 0.01, 0.1, or 1.0 M sodium sulfite). PO_2 in the microfluidic channel was successively lowered by increasing the concentration of sulfite in the O_2 sink (0.0–1.0 M). RBC motion was captured by a high-speed camera. w, width.

(B) Left: to colorimetrically quantify PO_2 in the capillary channel, we prepared 25 μM of tris(2,2′-bipyridyl)dichlororuthenium(II) hexahydrate in N_2-bubbled de-ionized (DI) water (n = 3) and in air-saturated DI water (n = 4). The change in fluorescence intensity of the O_2 indicator dye solution flowing through the microfluidic device was measured during exposure to 0.0, 0.01, 0.1, 1.0, 1.5, and 2.0 M sodium sulfite solution and converted to PO_2. Right: images comparing RBC flow within an O_2 sink containing 0 or 1 M sulfite. Images of flowing RBCs captured by the high-speed camera at sequential time points are superimposed. T, time.

(legend continued on next page)

(Figure 4B). Remarkably, the velocity of RBCs flowing through the channel increased as a function of O_2 depletion, indicating that brief deoxygenation alone can affect the mechanical properties of RBCs (Figures 4B and 4C). The O_2-dependent increase in RBC velocity was observed when RBCs were resuspended in either plasma or PBS (Figure 4C). Because PO_2 in capillaries is highly variable and can range from ~5 to 95 mmHg but tends to be on the lower end of that range within true microvessels (Kasischke et al., 2011; Parpaleix et al., 2013; Sakadžić et al., 2014), we focused on the effects of relatively lower PO_2. In these experiments, the PBS was first purged with N_2 until the PO_2 reached 34 mmHg, approximating normal brain PO_2 (Jaeger et al., 2005). Similar to above, RBCs were driven through a microfluidic chamber immersed in a sulfite sink (0 to 1 M) and colorimetrically calibrated (Figure 4B). This analysis showed that at a relatively lower range of O_2 tension, RBC velocities became more sensitive to surrounding changes in PO_2 ($p < 0.001$, t test with Bonferroni test, compared to PBS without N_2 purging and plasma) (Figures 4C and 4D). Interestingly, however, increasing the O_2 from 21% to 100% (or from PO_2 ~160 mmHg to ~760 mmHg) failed to alter RBC velocity in the microfluidic capillary (1.000 normalized velocity in 21% versus 0.998 normalized velocity in 100% O_2, $n = 9–19$, $p > 0.05$, t test), consistent with the notion that at supraphysiologic PO_2, hemoglobin continues to be maximally saturated with O_2 and RBCs reach the limit of their ability to bind additional O_2 and respond with velocity changes. Classical studies have shown that in response to deoxygenation and/or mechanical stress, RBCs release ATP, which activates endothelial cell purinergic receptors (P_2YR1s), resulting in NO release. In turn, NO or other endothelium-dependent vasodilators increase blood flow in hypoxic tissues via arterial smooth muscle relaxation (Chen et al., 2014; Ellsworth et al., 2009; Jia et al., 1996). RBCs may also directly release NO from S-nitroso-Hb upon deoxygenation (Jensen, 2009). However, we found that the PO_2-elicited increase in RBC flow velocity was not a result of direct ATP or NO release. Exposing RBCs to the ATP-degrading enzyme apyrase (40 U/mL) or the NO synthase inhibitor L-NAME (3 mM) did not affect PO_2-induced elevations in RBC velocity (Figure 4D), in accordance with the in vivo observation that L-NAME failed to suppress capillary hyperemia (Figure 2G). In addition, CNQX had no effect on PO_2-induced increases in RBC velocity through the microfluidic channel (Figure 4D). When RBCs were treated with K^+ channel inhibitors (4-aminopyridine [4-AP, non-selective voltage-dependent K^+ channel blocker, 1 mM], charybdotoxin [Ca^{2+}-activated voltage-gated K^+ channel blocker, 100 nM], or iberiotoxin [large-conductance Ca^{2+}-activated K^+ channel blocker, 100 nM]), however, the sensitivity of RBC velocity to PO_2 changes decreased (Figure 4E), suggesting that K^+ flux across the membrane plays a role in the velocity of RBC flow in capillaries. As a negative control, RBCs were treated with diamide, which stiffens the RBC membrane by crosslinking the cytoskeletal spectrin network (Fischer et al., 1978; Wan et al., 2008). The flow velocity of diamide-exposed RBCs was unaffected by PO_2, supporting the notion that the PO_2-induced increase in RBC flow velocity is due to increased deformability of the RBC membrane (Figure 4D).

To directly test whether RBC deformability is controlled by PO_2, we assessed the shear-induced deformability of RBCs flowing in a relatively large-sized microfluidic channel containing a segment of constriction (width = 20 μm) (Figure 4F). The shear-induced deformability of RBCs was characterized by the elongation index D_L/D_W, where D_L and D_W represented the length and thickness of an RBC flowing through the constriction, respectively (adapted from Forsyth et al., 2010; Mohandas et al., 1980). We found that the elongation of RBCs in response to shear stress increased as PO_2 decreased, demonstrating that RBCs are more flexible in lower PO_2 conditions (Figure 4G). The dependence of RBC deformability on PO_2 was significantly diminished when diamide was added (Figure 4G). RBCs treated with the K^+ channel blockers 4-AP (1 mM), charybdotoxin (100 nM), or iberiotoxin (100 nM) also exhibited reduced sensitivity to PO_2 changes compared to controls (Figure 4H). These data show that lowering PO_2 increases RBC deformability and thereby the velocity by which RBCs pass through a narrow ex vivo capillary lacking endothelial cells, pericytes, and astrocytes. Exposure to K^+ channel inhibitors reduced the

(C) Lowering PO_2 in the microfluidic channel caused an increase in RBC velocity. Responsiveness of RBCs to surrounding PO_2 levels did not differ regardless of resuspension in PBS ($n = 214$, RBC velocity [mm/s] = $-0.137 \times PO_2$ [mmHg] + 80.056, $R^2 = 0.910$) or plasma ($n = 42$, RBC velocity [mm/s] = $-0.157 \times PO_2$ [mmHg] + 69.069, $R^2 = 0.995$). $p > 0.05$, t test with Bonferroni test.

(D) The starting PO_2 in the PBS bath was lowered to 34 mmHg by N_2 purging prior to immersion in the O_2 sink, and RBC velocity continued to be sensitive to surrounding PO_2 changes ($n = 71$, RBC velocity [mm/s] = $-0.451 \times PO_2$ [mmHg] + 82.074, $R^2 = 0.999$). Dephosphorylation of extracellular ATP by apyrase (40 U/mL) or inhibition of NOS and AMPA receptors by L-NAME (3 mM) and CNQX (200 μM), respectively, did not alter RBC velocity increases in response to lowering surrounding PO_2. $n = 5–74$. $p > 0.05$, one-way ANOVA. When diamide (200 μM) was added to stiffen RBC membranes, lowering PO_2 failed to increase RBC velocity compared to controls. $n = 70–71$. $p < 0.0001$, t test.

(E) In the presence of the potassium channel inhibitors 4-aminopyridine (4-AP) (1 mM) ($n = 199$, RBC velocity [mm/s] = $-0.299 \times PO_2$ [mmHg] + 82.304, $R^2 = 0.992$), charybdotoxin (100 nM) ($n = 197$, RBC velocity [mm/s] = $-0.278 \times PO_2$ [mmHg] + 82.277, $R^2 = 0.993$), or iberiotoxin (100 nM) ($n = 188$, RBC velocity [mm/s] = $-0.213 \times PO_2$ [mmHg] + 78.011, $R^2 = 0.944$), the sensitivity of RBC velocity to the change in PO_2 was reduced. $n = 188–199$. $p < 0.05$, one-way ANOVA.

(F) A schematic of the experimental setup for ex vivo analysis of the effect of PO_2 on RBC deformability. RBCs suspended in a N_2-purged PBS solution were injected into a microfluidic device containing a constriction (width = 20 μm) and constant pressure (1.6 psi) was applied. The microfluidic device was submerged in an O_2 sink similar to Figure 4A, and RBC motion was captured by a high-speed camera. The deformability of RBCs was characterized by the elongation index D_L/D_W, where D_L and D_W represent the length and thickness of a RBC flowing through the constriction.

(G) The elongation index (D_L/D_W) of RBCs increased with a decrease in surrounding O_2 levels for control RBCs ($n = 239$, RBC $D_L/D_W = -0.0237 \times PO_2$ [mmHg] + 4.0886, $R^2 = 0.993$). Compared to control RBCs flowing through the channel, diamide-treated (200 μM) RBCs did not deform significantly in response to changes in PO_2. $n = 88–239$. $p < 0.0001$, t test.

(H) Elongation indexes (D_L/D_W) of control RBCs and RBCs treated with 4-AP (1 mM) ($n = 276$, RBC $D_L/D_W = -0.0373 \times PO_2$ [mmHg] + 4.0224, $R^2 = 0.997$), charybdotoxin (100 nM) ($n = 256$, RBC $D_L/D_W = -0.0386 \times PO_2$ [mmHg] + 4.0795, $R^2 = 0.992$), or iberiotoxin (100 nM) ($n = 208$, RBC $D_L/D_W = -0.0377 \times PO_2$ [mmHg] + 4.0085, $R^2 = 0.992$) at different O_2 tensions are shown. $n = 208–276$. $p < 0.05$, one-way ANOVA.

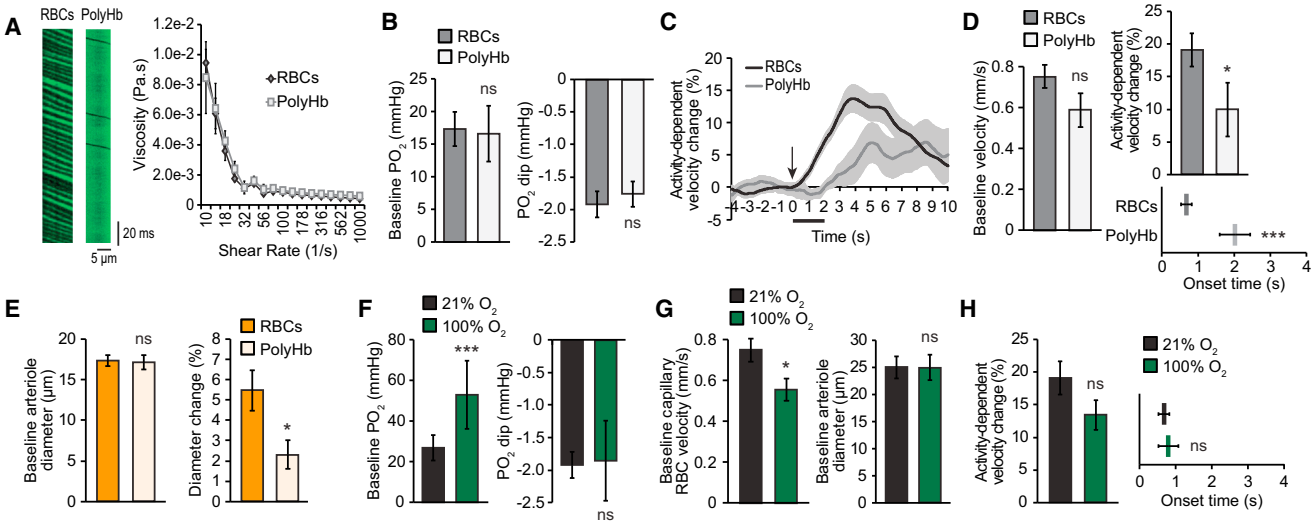

Figure 5. Oxygen Carriage by Erythrocytes Is Required for Functional Hyperemia

(A) Left: capillary line-scan images from a control and PolyHb-exchanged mouse. Right: PolyHb blood exchange does not alter blood viscosity.

(B) Left: baseline tissue PO_2 is unchanged by PolyHb blood exchange (17.31 ± 2.62 mmHg in controls, 16.59 ± 4.27 mmHg in PolyHb). n = 7–14 mice. ns, $p > 0.05$, Mann-Whitney test. Right: PO_2 dip in response to hindlimb stimulation is similar between mice with and without PolyHb blood exchange (1.92 ± 0.20 mmHg PO_2 dip in controls, 1.76 ± 0.20 mmHg PO_2 dip in PolyHb). n = 36–47, 6–21 mice. ns, $p > 0.05$, Mann-Whitney test.

(C) Capillary RBC velocity responses during hindlimb stimulation in mice with PolyHb blood replacement. Black arrow indicates start of stimulation, black bar indicates duration of stimulation.

(D) Left: baseline capillary RBC velocity in mice with (0.59 ± 0.08 mm/s) and without (0.75 ± 0.06 mm/s) PolyHb blood exchange. n = 23–65, 8–25 mice. ns, $p > 0.05$, Mann-Whitney test. Right: comparison of capillary RBC velocity increases in response to hindlimb stimulation (19.15% ± 2.57% in controls, 9.97% ± 4.15% in PolyHb). Onset time of capillary velocity changes (0.67 ± 0.15 s in controls, 2.02 ± 0.42 s in PolyHb). n = 23–65, 8–25 mice. *$p < 0.05$, Mann-Whitney test, ***$p < 0.001$, t test.

(E) Left: baseline arteriole diameter in mice with (17.14 ± 0.85 μm) and without (17.40 ± 0.68 μm) PolyHb blood exchange. n = 32–53, 6–18 mice. ns, $p > 0.05$, t test. Right: percentage of evoked arteriole vasodilation in mice with (2.30% ± 0.71%) and without (5.47% ± 0.99%) PolyHb blood exchange. n = 32–53, 6–18 mice. *$p < 0.05$, Mann-Whitney test.

(F) Left: inspired 100% O_2 increases baseline brain parenchymal PO_2 (26.80 ± 6.24 mmHg PO_2 in room air, 52.89 ± 16.75 mmHg PO_2 in 100% O_2). n = 15 mice. ***$p < 0.001$, Wilcoxon test. Right: hindlimb stimulation-induced PO_2 dips were preserved in mice ventilated with 100% O_2 (1.92 ± 0.20 mmHg PO_2 dip in room air, 1.86 ± 0.61 mmHg PO_2 dip in 100% O_2). n = 14–47, 10–21 mice. ns, $p > 0.05$, Mann-Whitney test.

(G) Left: baseline capillary RBC velocity in mice ventilated with room air and 100% O_2 (0.75 ± 0.06 mm/s in room air, 0.56 ± 0.05 mm/s in 100% O_2). n = 32–65, 11–25 mice. *$p < 0.05$, Mann-Whitney test. Right: baseline cortical arteriole diameter in mice ventilated with room air and 100% O_2 (24.96 ± 2.06 μm in room air, 24.94 ± 2.34 μm in 100% O_2). n = 10, 3 mice. ns, $p > 0.05$, paired t test.

(H) Left: hindlimb stimulation-evoked capillary RBC velocity increases (19.15% ± 2.57% in room air, 13.44% ± 2.25% in 100% O_2). n = 32–65, 11–25 mice. ns, $p > 0.05$, Mann-Whitney test. Right: onset time of capillary RBC velocity changes (0.67 ± 0.15 s in room air, 0.79 ± 0.27 s in 100% O_2). n = 32–65, 11–25 mice. ns, $p > 0.05$, Mann-Whitney test. Data are represented as mean ± SEM.

deformability of RBCs and thus the potency by which PO_2 increased RBC flow velocity. This latter observation is consistent with prior studies documenting that a decrease in cell volume mediated by K^+ efflux and water loss may play a role in permitting RBC deformation during the shear stress associated with squeezing through a narrow capillary (Cinar et al., 2015).

Exchanging RBCs for an O_2-Carrying Blood Substitute Suppresses Functional Hyperemia In Vivo

Our ex vivo data suggest that RBCs autonomously regulate their own velocities through capillaries in response to changes in surrounding PO_2 tension. If this finding is relevant in vivo, we would expect that in vivo capillary hyperemia is suppressed when RBCs are replaced by an acellular hemoglobin-based O_2 carrier (HBOC). To meticulously test whether RBCs are required for activity-dependent capillary hyperemia, we partially exchanged the blood in our mouse model with a synthetic HBOC, i.e., polymerized hemoglobin (PolyHb) (Baek et al., 2012; Zhou et al., 2011). We were able to decrease the hematocrit by 80.3% ± 0.5% (10.55 ± 0.11 × 10^6 versus 2.08 ± 0.046 × 10^6 cells per μL) by gradually replacing RBCs with PolyHb. Mixing PolyHb with whole blood did not alter blood viscosity (Figure 5A). PolyHb blood exchange did not alter resting cortical PO_2, sensory-induced dips in PO_2 (Figure 5B), or sensory-evoked electrical activity (evoked LFP 10 Hz power was 0.017 ± 0.0085 mV^2 in control mice and 0.015 ± 0.0064 mV^2 in PolyHb mice, $p > 0.05$, t test). It did, however, delay the onset time and reduce the amplitude of activity-dependent capillary hyperemia (Figures 5C and 5D). Basal cortical arteriole diameters were unchanged but evoked arteriole vasodilation was reduced with PolyHb (Figure 5E). With an insufficient RBC population, capillary hyperemia may be primarily driven by upstream arteriole vasodilation.

How does hyperoxygenation affect the microcirculation? Breathing 100% O_2 elevated baseline cortical PO_2 from ~25 to

~50 mmHg (Jaeger et al., 2005) without causing significant changes in the evoked PO_2 dip (Figure 5F). Basal capillary RBC velocities were reduced while basal arteriole diameters and capillary hyperemia were unchanged (Figures 5G and 5H). Hence, both the ex vivo and in vivo observations provide strong support for the notion that deoxygenation-mediated changes in erythrocyte deformability drive capillary hyperemia.

DISCUSSION

Despite the uncontested tight linkage between neural activity and vascular responses, the question of what drives functional hyperemia is still debated. In principle, a mechanism sensing depletion of an energy substrate (O_2 or glucose) or alternatively the release of vasoactive mediators (NO, PGE_2, ATP, adenosine, K^+, and other molecules) could drive activity-dependent increases in blood flow. In this work, we took advantage of the discovery that functional hyperemia is initiated in microvessels rather than in arterioles (Hall et al., 2014). We confirmed that capillary RBC velocity increases 1–2 s prior to arterial hyperemia but similar to a recent study (Hill et al., 2015) failed to identify pericytes as the principal regulator of capillary hyperemia. Several experimental findings presented here implicate the transient PO_2 dip in the initiation of the activity-dependent increase in capillary perfusion via a mechanism independent of the release of vasoactive agents and smooth muscle relaxation, including: (1) capillary functional hyperemia was suppressed when oxidative metabolism was inhibited by local application of NaCN. Not only does this observation support the notion that PO_2 regulates capillary perfusion, but it also indirectly provides evidence against a central role of vasoactive mediators in initiating functional hyperemia, since adenosine, lactate, and K^+ release are all increased when oxidative metabolism is inhibited (Daval et al., 1980). (2) The AMPA receptor blocker CNQX suppressed the spontaneous fluctuations in resting PO_2 and capillary RBC velocity by 45.0% and 26.7%, respectively, indicating that AMPA receptor activity in part drives spontaneous changes in O_2 tension and capillary RBC flow. Moreover, activity-induced PO_2 dips (90.1%) and capillary hyperemia (75.0%) were both potently suppressed by CNQX. (3) Microinjection of O_2 scavengers induced capillary hyperemia in the absence of an increase in neural activity. The hyperemia induced by local scavenging of O_2 was not suppressed by antagonists of adenosine A1 and A2A receptors or inhibitors of K^+ channels, NO and PGE_2 production, or O_2 consumption (NaCN). (4) Ex vivo quantification of the velocity of RBCs moving through a microfluidic channel under strict PO_2 control showed that RBC velocity increased as a direct function of physiologically relevant decreases in PO_2. Transient manipulation of PO_2 within the range of 0–160 mmHg directly controlled not only the velocity by which RBCs traveled through a narrow synthetic channel in the absence of endothelial cells, pericytes, and astrocytes but also RBC deformability in response to shear stress. In contrast, elevation of PO_2 (100% O_2) considerably past physiologic levels failed to decrease RBC velocity beyond what was observed in room air (~21% O_2). (5) Partial replacement of intravascular RBCs with a synthetic RBC-free blood substitute in vivo showed that lowering the hematocrit by ~80% was associated with a significant reduction in activity-dependent capillary hyperemia. Together, these observations provide evidence to support the novel concept that RBCs are not only sensors of PO_2 but can also regulate their deformability and thereby the velocity with which they pass through capillaries in response to transient drops in tissue oxygenation.

The effect of PO_2 on RBC deformability is debated, possibly because most past studies were based on indirect measurements that have not been readily reproducible (Kim et al., 2015; Martindale and McKay, 1995; Yoon et al., 2009). To our knowledge, no prior studies have directly quantified changes in RBC velocity and deformability in response to *transient* changes in PO_2. The data presented here using an ex vivo microfluidic approach demonstrate a direct relationship between RBC velocity and deformability elicited by transient decreases in PO_2.

Deoxygenation of RBCs leads to displacement of ankyrin from band 3, resulting in release of the spectrin/actin cytoskeleton from the cell membrane (Stefanovic et al., 2013). The weakening of membrane-cytoskeletal interactions has been proposed to be beneficial to blood flow during brief periods of deoxygenation (Stefanovic et al., 2013) and may contribute to increased RBC deformability during drops in PO_2. Prior studies in peripheral tissues have shown that RBCs can induce hyperemia but pointed to a mechanism that involves ATP release from RBCs (under shear-induced deformation and/or hypoxia), which triggers endothelial cell NO production that subsequently dilates arteries by hyperpolarizing vascular smooth muscle cells (Ellsworth et al., 2009). Our microfluidic chamber experiments showing that lowering PO_2 in the absence of the neurovascular unit increased isolated RBC velocity, coupled with the finding that L-NAME (an inhibitor of NO synthase) had no effect on capillary hyperemia, argue against a significant contribution from this paracellular signaling mechanism. Furthermore, PO_2-induced arteriole dilation was delayed relative to PO_2-induced capillary blood flow increases, mimicking hyperemia elicited by sensory input and signifying that arteriole vasodilation is not the primary driver of PO_2-dependent capillary hyperemia. Previously, the existence of an O_2-sensing mechanism has been questioned based on the finding that regional functional hyperemia persisted in hyperbaric hyperoxia (Lindauer et al., 2010). We here confirmed that capillary hyperemia was preserved in hyperoxia but extended the analysis to show that activity-induced PO_2 dips persisted during hyperoxic conditions. Thus, hyperoxia did not suppress either activity-induced PO_2 dips or capillary hyperemia. Additionally, inhibiting metabolic O_2 consumption by application of cyanide blocked both activity-dependent dips in PO_2 and capillary hyperemia irrespective of the baseline tissue PO_2. Collectively, these sets of data suggest that it is the transient PO_2 dip rather than baseline PO_2 that triggers capillary hyperemia. This conclusion is further supported by our ex vivo observation that RBC velocity in the microfluidic device increased in response to PO_2 reductions across a wide range of physiological PO_2 levels (0–160 mmHg).

It is important to note that functional hyperemia outlasted the dip in PO_2. Accordingly, only the very initial phase (<1.5 s) of capillary hyperemia that precedes arterial dilation is driven by activity-induced dips in PO_2. The initial capillary response during functional hyperemia may serve as the rapid phase of hyperemia

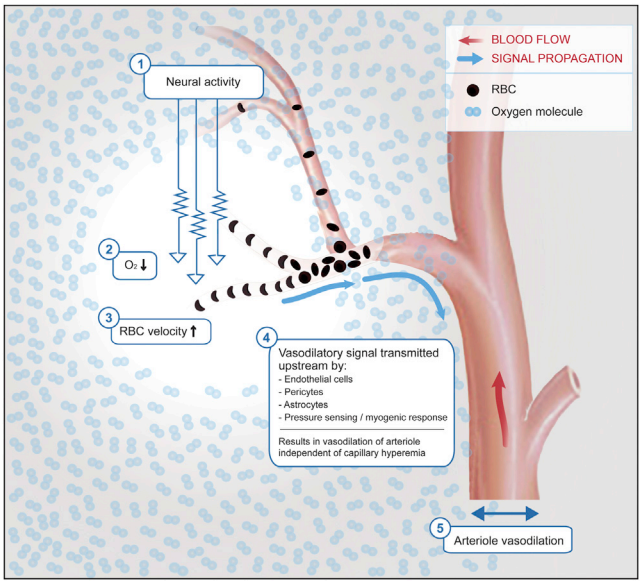

Figure 6. Model of Capillary Hyperemia and Potential Link to Upstream Arteriole Dilation

(1) Sensory input triggers local neural activation resulting in (2) a local dip in tissue and plasma O_2 tension (Parpaleix et al., 2013). The dip in plasma O_2 tension changes the mechanical properties of RBCs resulting in (3) an increase in RBC velocity. The transient dip in O_2 tension drives the fast, initial phase of capillary hyperemia. The rise in RBC velocity in both capillaries and arterioles rapidly increases O_2 delivery, resulting in an O_2 overshoot (4 and 5). The delayed and more sustained phase of capillary hyperemia is driven by vasodilation of upstream arterioles. It is not known whether the initial phase of capillary hyperemia, which is driven by a dip in local PO_2, is mechanistically linked to the delayed dilation of the upstream arteriole. Hypothetical pathways of signal propagation along the neurovascular unit include Ca^{2+} signaling in endothelial cells, pericytes, or vascular endfeet of astrocytes. Also, it is possible that an initial increase in capillary perfusion results in pressure changes that trigger a myogenic response in the upstream arteriole. Finally, capillary hyperemia and arteriole vasodilation may be initiated independently. Several mechanisms, including release of vasoactive mediators from interneurons or astrocytes, are known to directly cause arteriole vasodilation (Cauli and Hamel, 2010; Iadecola and Nedergaard, 2007).

that supplies active neurons with immediately available O_2. The delayed and sustained hyperemic phase is most likely powered by the slower dilation of upstream arterioles and serves to prevent a prolonged drop in oxygenation at tissue located more remotely from arterioles and proximal capillaries (Devor et al., 2011; Leithner and Royl, 2014). It is unclear whether PO_2-mediated rapid capillary hyperemia directly causes delayed arteriole vasodilation, as it has been shown that release of vasoactive agents from both interneurons and astrocytes can trigger arteriole dilation (Cauli and Hamel, 2010; Takano et al., 2006). Capillary hyperemia and arteriole hyperemia may have independent regulatory mechanisms that work in a concerted manner to optimize blood supply. Alternatively, the delayed dilation of upstream arterioles may be a consequence of PO_2-induced rapid capillary hyperemia, mediated by the propagation of Ca^{2+} signals along the neurovascular unit (Figure 6). If so, it is interesting to speculate whether the impaired vasoreactivity observed in various diseases and in aging is a consequence of impaired PO_2-mediated capillary hyperemia. Future studies can address the relationship between capillary hyperemia and delayed arteriole dilation. Further experiments can also assess sensory-evoked capillary hyperemia in awake behaving mice.

Functional hyperemia is an integrated response that tightly couples O_2 consumption with O_2 supply. Here we show that both spontaneous and activity-induced dips in tissue PO_2 drive the earliest phase of capillary hyperemia. Furthermore, PO_2 directly controls the velocity by which RBCs transit through a narrow channel in a microfluidic device. Thus, RBCs may themselves serve as autonomous regulators of capillary perfusion that operate independently of the neurovascular unit and the release of vasoactive molecules. The idea that erythrocytes—the major suppliers of O_2—function not only as O_2 carriers but also as O_2 sensors and regulators of capillary blood flow provides a simple, yet swift and precise, mechanism for controlling the cerebral microcirculation.

EXPERIMENTAL PROCEDURES

Animals

C57Bl6 mice (25–30 g, 8–12 weeks old, The Jackson Laboratory) and NG2-DsRed mice (Tg(Cspg4-DsRed.T1)1Akik/J, RRID: IMSR_JAX:008241) (Zhu et al., 2008) on a C57Bl6 background of either sex were utilized. Mice were prepared for in vivo imaging as described previously (Bekar et al., 2008; Ding et al., 2013; Wang et al., 2006; Xie et al., 2013) and in the Supplemental Experimental Procedures.

Physiological Manipulations and Measurements

Physiological manipulations and measurements were performed as previously described (Baek et al., 2012; Bekar et al., 2012; Kasischke et al., 2011; Takano et al., 2007; Vázquez et al., 2011; Xie et al., 2013; Zhou et al., 2011) and in the Supplemental Experimental Procedures.

Microfluidic Device and RBC Imaging

Microfluidic device construction and human RBC imaging were performed as previously described (Duffy et al., 1998; Wan et al., 2008, 2011) and in the Supplemental Experimental Procedures.

Intrinsic Optical Signal and Two-Photon Imaging

Intrinsic optical signaling (IOS), two-photon imaging, and immunofluorescence imaging were performed as previously described (Armulik et al., 2011; Bekar et al., 2012) and in the Supplemental Experimental Procedures.

Statistics

All data were expressed as mean ± SEM. Normality of the data was evaluated with the Shapiro-Wilk test, and non-parametric tests were used when normality was not assumed. A Student's t test or Mann-Whitney test was used to compare two groups. A one-way ANOVA with a Bonferroni's multiple comparison test or a Kruskal-Wallis test with a Dunn's multiple comparison test was used to compare multiple groups. A paired t test or Wilcoxon matched-pairs signed-rank test was used for pairwise comparisons. $p < 0.05$ was considered significant.

SUPPLEMENTAL INFORMATION

Supplemental Information includes Supplemental Experimental Procedures and three figures and can be found with this article online at http://dx.doi.org/10.1016/j.neuron.2016.07.016.

AUTHOR CONTRIBUTIONS

Conceptualization, M.N., J.W., and H.S.W.; Methodology, H.S.W., H.K., I.D.R., N.L., and S.Z.; Software, I.D.R. and H.S.W.; Investigation, M.N., J.W., H.S.W.,

H.K., N.L., S.Z., Y.W., E.D.M., and A.G.; Resources, A.F.P., K.E.R., and C.X.; Writing – Original Draft, M.N., J.W., and H.S.W.; Writing – Review & Editing, M.N., J.W., H.S.W., S.Z., A.F.P., and I.D.R.; Visualization, M.N., J.W., H.S.W., and S.Z.; Supervision, M.N. and J.W.; Funding Acquisition, M.N. and J.W.

ACKNOWLEDGMENTS

This study was supported by the NIH/NINDS, Novo Nordisk, the European Union's Horizon 2020 research and innovation program under grant agreement No. 666881 SVDs@target, and Rochester Institute of Technology. We thank Takahiro Takano, Lulu Xie, Wei Song, Priyanka Pillai, Prishanya Pillai, Jordana Schmierer, and Katherine Reitz for expert technical assistance and Dan Xue for assistance with illustrations.

Received: July 17, 2015
Revised: May 11, 2016
Accepted: June 26, 2016
Published: August 4, 2016

REFERENCES

Abkarian, M., Faivre, M., and Stone, H.A. (2006). High-speed microfluidic differential manometer for cellular-scale hydrodynamics. Proc. Natl. Acad. Sci. USA *103*, 538–542.

Armulik, A., Genové, G., and Betsholtz, C. (2011). Pericytes: developmental, physiological, and pathological perspectives, problems, and promises. Dev. Cell *21*, 193–215.

Baek, J.H., Zhou, Y., Harris, D.R., Schaer, D.J., Palmer, A.F., and Buehler, P.W. (2012). Down selection of polymerized bovine hemoglobins for use as oxygen releasing therapeutics in a guinea pig model. Toxicol. Sci. *127*, 567–581.

Bekar, L., Libionka, W., Tian, G.F., Xu, Q., Torres, A., Wang, X., Lovatt, D., Williams, E., Takano, T., Schnermann, J., et al. (2008). Adenosine is crucial for deep brain stimulation-mediated attenuation of tremor. Nat. Med. *14*, 75–80.

Bekar, L.K., Wei, H.S., and Nedergaard, M. (2012). The locus coeruleus-norepinephrine network optimizes coupling of cerebral blood volume with oxygen demand. J. Cereb. Blood Flow Metab. *32*, 2135–2145.

Cauli, B., and Hamel, E. (2010). Revisiting the role of neurons in neurovascular coupling. Front. Neuroenergetics *2*, 9.

Chaigneau, E., Oheim, M., Audinat, E., and Charpak, S. (2003). Two-photon imaging of capillary blood flow in olfactory bulb glomeruli. Proc. Natl. Acad. Sci. USA *100*, 13081–13086.

Chen, B.R., Kozberg, M.G., Bouchard, M.B., Shaik, M.A., and Hillman, E.M. (2014). A critical role for the vascular endothelium in functional neurovascular coupling in the brain. J. Am. Heart Assoc. *3*, e000787.

Cinar, E., Zhou, S., DeCourcey, J., Wang, Y., Waugh, R.E., and Wan, J. (2015). Piezo1 regulates mechanotransductive release of ATP from human RBCs. Proc. Natl. Acad. Sci. USA *112*, 11783–11788.

Daval, J.L., Barberis, C., and Gayet, J. (1980). Release of [14C]adenosine derivatives from superfused synaptosome preparations. Effects of depolarizing agents and metabolic inhibitors. Brain Res. *181*, 161–174.

Devor, A., Sakadzic, S., Saisan, P.A., Yaseen, M.A., Roussakis, E., Srinivasan, V.J., Vinogradov, S.A., Rosen, B.R., Buxton, R.B., Dale, A.M., and Boas, D.A. (2011). "Overshoot" of O_2 is required to maintain baseline tissue oxygenation at locations distal to blood vessels. J. Neurosci. *31*, 13676–13681.

Ding, F., O'Donnell, J., Thrane, A.S., Zeppenfeld, D., Kang, H., Xie, L., Wang, F., and Nedergaard, M. (2013). α1-Adrenergic receptors mediate coordinated Ca2+ signaling of cortical astrocytes in awake, behaving mice. Cell Calcium *54*, 387–394.

Duffy, D.C., McDonald, J.C., Schueller, O.J., and Whitesides, G.M. (1998). Rapid prototyping of microfluidic systems in Poly(dimethylsiloxane). Anal. Chem. *70*, 4974–4984.

Ellsworth, M.L., Ellis, C.G., Goldman, D., Stephenson, A.H., Dietrich, H.H., and Sprague, R.S. (2009). Erythrocytes: oxygen sensors and modulators of vascular tone. Physiology (Bethesda) *24*, 107–116.

Enager, P., Piilgaard, H., Offenhauser, N., Kocharyan, A., Fernandes, P., Hamel, E., and Lauritzen, M. (2009). Pathway-specific variations in neurovascular and neurometabolic coupling in rat primary somatosensory cortex. J. Cereb. Blood Flow Metab. *29*, 976–986.

Fischer, T.M., Haest, C.W., Stöhr, M., Kamp, D., and Deuticke, B. (1978). Selective alteration of erythrocyte deformabiliby by SH-reagents: evidence for an involvement of spectrin in membrane shear elasticity. Biochim. Biophys. Acta *510*, 270–282.

Forsyth, A.M., Wan, J., Ristenpart, W.D., and Stone, H.A. (2010). The dynamic behavior of chemically "stiffened" red blood cells in microchannel flows. Microvasc. Res. *80*, 37–43.

Girouard, H., and Iadecola, C. (2006). Neurovascular coupling in the normal brain and in hypertension, stroke, and Alzheimer disease. J. Appl. Physiol. *100*, 328–335.

Hall, C.N., Reynell, C., Gesslein, B., Hamilton, N.B., Mishra, A., Sutherland, B.A., O'Farrell, F.M., Buchan, A.M., Lauritzen, M., and Attwell, D. (2014). Capillary pericytes regulate cerebral blood flow in health and disease. Nature *508*, 55–60.

Hill, R.A., Tong, L., Yuan, P., Murikinati, S., Gupta, S., and Grutzendler, J. (2015). Regional blood flow in the normal and ischemic brain is controlled by arteriolar smooth muscle cell contractility and not by capillary pericytes. Neuron *87*, 95–110.

Hoffmeyer, H.W., Enager, P., Thomsen, K.J., and Lauritzen, M.J. (2007). Nonlinear neurovascular coupling in rat sensory cortex by activation of transcallosal fibers. J. Cereb. Blood Flow Metab. *27*, 575–587.

Iadecola, C., and Nedergaard, M. (2007). Glial regulation of the cerebral microvasculature. Nat. Neurosci. *10*, 1369–1376.

Jaeger, M., Soehle, M., and Meixensberger, J. (2005). Brain tissue oxygen (PtiO2): a clinical comparison of two monitoring devices. Acta Neurochir. Suppl. (Wien) *95*, 79–81.

Jensen, F.B. (2009). The dual roles of red blood cells in tissue oxygen delivery: oxygen carriers and regulators of local blood flow. J. Exp. Biol. *212*, 3387–3393.

Jia, L., Bonaventura, C., Bonaventura, J., and Stamler, J.S. (1996). S-nitrosohaemoglobin: a dynamic activity of blood involved in vascular control. Nature *380*, 221–226.

Kasischke, K.A., Lambert, E.M., Panepento, B., Sun, A., Gelbard, H.A., Burgess, R.W., Foster, T.H., and Nedergaard, M. (2011). Two-photon NADH imaging exposes boundaries of oxygen diffusion in cortical vascular supply regions. J. Cereb. Blood Flow Metab. *31*, 68–81.

Kim, J., Le, H., and Shin, S. (2015). Advances in the measurement of red blood cell deformability: a brief review. J. Cell. Biotechnol. *1*, 63–79.

Kleinfeld, D., Mitra, P.P., Helmchen, F., and Denk, W. (1998). Fluctuations and stimulus-induced changes in blood flow observed in individual capillaries in layers 2 through 4 of rat neocortex. Proc. Natl. Acad. Sci. USA *95*, 15741–15746.

Kleinfeld, D., Blinder, P., Drew, P.J., Driscoll, J.D., Muller, A., Tsai, P.S., and Shih, A.Y. (2011). A guide to delineate the logic of neurovascular signaling in the brain. Front. Neuroenergetics *3*, 1.

Kornfield, T.E., and Newman, E.A. (2014). Regulation of blood flow in the retinal trilaminar vascular network. J. Neurosci. *34*, 11504–11513.

Lecoq, J., Parpaleix, A., Roussakis, E., Ducros, M., Goulam Houssen, Y., Vinogradov, S.A., and Charpak, S. (2011). Simultaneous two-photon imaging of oxygen and blood flow in deep cerebral vessels. Nat. Med. *17*, 893–898.

Leithner, C., and Royl, G. (2014). The oxygen paradox of neurovascular coupling. J. Cereb. Blood Flow Metab. *34*, 19–29.

Lindauer, U., Leithner, C., Kaasch, H., Rohrer, B., Foddis, M., Füchtemeier, M., Offenhauser, N., Steinbrink, J., Royl, G., Kohl-Bareis, M., and Dirnagl, U. (2010). Neurovascular coupling in rat brain operates independent of hemoglobin deoxygenation. J. Cereb. Blood Flow Metab. *30*, 757–768.

Martindale, V.E., and McKay, K. (1995). Hyperbaric oxygen treatment of dogs has no effect on red cell deformability but causes an acute fluid shift. Physiol. Chem. Phys. Med. NMR *27*, 45–53.

Mathiesen, C., Caesar, K., Thomsen, K., Hoogland, T.M., Witgen, B.M., Brazhe, A., and Lauritzen, M. (2011). Activity-dependent increases in local oxygen consumption correlate with postsynaptic currents in the mouse cerebellum in vivo. J. Neurosci. *31*, 18327–18337.

Mohandas, N., Clark, M.R., Jacobs, M.S., and Shohet, S.B. (1980). Analysis of factors regulating erythrocyte deformability. J. Clin. Invest. *66*, 563–573.

Parpaleix, A., Goulam Houssen, Y., and Charpak, S. (2013). Imaging local neuronal activity by monitoring PO_2 transients in capillaries. Nat. Med. *19*, 241–246.

Petzold, G.C., and Murthy, V.N. (2011). Role of astrocytes in neurovascular coupling. Neuron *71*, 782–797.

Sakadžić, S., Mandeville, E.T., Gagnon, L., Musacchia, J.J., Yaseen, M.A., Yucel, M.A., Lefebvre, J., Lesage, F., Dale, A.M., Eikermann-Haerter, K., et al. (2014). Large arteriolar component of oxygen delivery implies a safe margin of oxygen supply to cerebral tissue. Nat. Commun. *5*, 5734.

Santisakultarm, T.P., Cornelius, N.R., Nishimura, N., Schafer, A.I., Silver, R.T., Doerschuk, P.C., Olbricht, W.L., and Schaffer, C.B. (2012). In vivo two-photon excited fluorescence microscopy reveals cardiac- and respiration-dependent pulsatile blood flow in cortical blood vessels in mice. Am. J. Physiol. Heart Circ. Physiol. *302*, H1367–H1377.

Self, M.W., Kooijmans, R.N., Supèr, H., Lamme, V.A., and Roelfsema, P.R. (2012). Different glutamate receptors convey feedforward and recurrent processing in macaque V1. Proc. Natl. Acad. Sci. USA *109*, 11031–11036.

Stefanovic, B., Hutchinson, E., Yakovleva, V., Schram, V., Russell, J.T., Belluscio, L., Koretsky, A.P., and Silva, A.C. (2008). Functional reactivity of cerebral capillaries. J. Cereb. Blood Flow Metab. *28*, 961–972.

Stefanovic, M., Puchulu-Campanella, E., Kodippili, G., and Low, P.S. (2013). Oxygen regulates the band 3-ankyrin bridge in the human erythrocyte membrane. Biochem. J. *449*, 143–150.

Takano, T., Tian, G.F., Peng, W., Lou, N., Libionka, W., Han, X., and Nedergaard, M. (2006). Astrocyte-mediated control of cerebral blood flow. Nat. Neurosci. *9*, 260–267.

Takano, T., Tian, G.F., Peng, W., Lou, N., Lovatt, D., Hansen, A.J., Kasischke, K.A., and Nedergaard, M. (2007). Cortical spreading depression causes and coincides with tissue hypoxia. Nat. Neurosci. *10*, 754–762.

Vázquez, B.Y., Hightower, C.M., Martini, J., Messmer, C., Frienesenecker, B., Corbels, P., Tsai, A.G., and Intaglietta, M. (2011). Vasoactive hemoglobin solution improves survival in hemodilution followed by hemorrhagic shock. Crit. Care Med. *39*, 1461–1466.

Wan, J., Ristenpart, W.D., and Stone, H.A. (2008). Dynamics of shear-induced ATP release from red blood cells. Proc. Natl. Acad. Sci. USA *105*, 16432–16437.

Wan, J., Forsyth, A.M., and Stone, H.A. (2011). Red blood cell dynamics: from cell deformation to ATP release. Integr Biol (Camb) *3*, 972–981.

Wang, X., Lou, N., Xu, Q., Tian, G.F., Peng, W.G., Han, X., Kang, J., Takano, T., and Nedergaard, M. (2006). Astrocytic Ca2+ signaling evoked by sensory stimulation in vivo. Nat. Neurosci. *9*, 816–823.

Xie, L., Kang, H., Xu, Q., Chen, M.J., Liao, Y., Thiyagarajan, M., O'Donnell, J., Christensen, D.J., Nicholson, C., Iliff, J.J., et al. (2013). Sleep drives metabolite clearance from the adult brain. Science *342*, 373–377.

Yacoub, E., Shmuel, A., Pfeuffer, J., Van De Moortele, P.F., Adriany, G., Ugurbil, K., and Hu, X. (2001). Investigation of the initial dip in fMRI at 7 Tesla. NMR Biomed. *14*, 408–412.

Yoon, Y.Z., Hong, H., Brown, A., Kim, D.C., Kang, D.J., Lew, V.L., and Cicuta, P. (2009). Flickering analysis of erythrocyte mechanical properties: dependence on oxygenation level, cell shape, and hydration level. Biophys. J. *97*, 1606–1615.

Zhou, Y., Jia, Y., Buehler, P.W., Chen, G., Cabrales, P., and Palmer, A.F. (2011). Synthesis, biophysical properties, and oxygenation potential of variable molecular weight glutaraldehyde-polymerized bovine hemoglobins with low and high oxygen affinity. Biotechnol. Prog. *27*, 1172–1184.

Zhu, X., Bergles, D.E., and Nishiyama, A. (2008). NG2 cells generate both oligodendrocytes and gray matter astrocytes. Development *135*, 145–157.